Photochemistry of Naphthalimide Photoacid Generators

Jean-Pierre Malval,[†] Shota Suzuki,[‡] Fabrice Morlet-Savary,[†] Xavier Allonas,*[,†] Jean-Pierre Fouassier,[†] Shigeru Takahara,[‡] and Tsuguo Yamaoka[‡]

Department of Photochemistry, UMR CNRS 7525, Université de Haute Alsace, ENSCMu 3 rue Alfred Werner, 68093 Mulhouse, France, and Department of Information and Image Science, Faculty of Engineering, Chiba University, 1-33 Yayoi-cho, Inage-ku, Chiba 263-8522, Japan

Received: September 7, 2007; In Final Form: February 4, 2008

The photophysical properties of a series of 1,8-naphthalimide photoacid generators were studied by steady state fluorescence and phosphorescence spectroscopy. Emission and excitation anisotropies, triplet quantum yields in polar and nonpolar solvent and photoacid generation were evaluated. The singlet excited state exhibits a low polarity and is strongly deactivated by an efficient intersystem crossing process. In protic solvent, a homolytic singlet cleavage of the N−O bond occurs and leads to the acid production. The existence of a triplet state close to the singlet state was clearly evidenced. The presence of close singlet excited states is supported by fluorescence anisotropy and picosecond laser spectroscopy experiments. Results of DFT calculations well confirm the experimental contentions and yield important information about the cleavage process involved in such compounds.

Introduction

Photoacid generator PAGs are the key materials in the field of photoresists for semiconductor fabrication. Since the concept of chemical amplification was presented for the first time, various kinds of ionic and nonionic PAGs as well as appropriate binder polymers bearing an acid-cleavable protection group[1−3] have been synthezised. Among the nonionic PAGs, iminosulfonate and imidosulfonate have attracted considerable attention as they have a N−O bond which is easily cleaved upon light irradiation.[4−8] Among them, 1,8-naphthalimide based photoacid generators bearing different kinds of substituents (Scheme 1) have been developed. Several aspects concerning the acid generation and the laser flash photolysis of some 1,8-naphthalimides derivatives have been already published.[4,7,9−11] However, very little is known about the excited state properties of compounds usable as PAG. The heterolytic vs the homolytic N−O bond cleavage was the subject of divergent opinions,[7,12] although no detailed mechanism was proposed. In a recent paper, we gave evidence for the homolytic cleavage and proposed a mechanism for the acid generation in the case of NIOTf.[13]

In the present paper, we will investigate the photophysical/photochemical properties of the particular naphtalimide compounds (NIs) shown in Scheme 1 such as: fluorescence, phosphorescence, triplet state T_1 generation, excited singlet state absorption, theoretical localization of the S_1 and T_1 state, acid formation, cleavage and photoacid generation mechanism in protic solvent (ethanol) or in the presence of residual water. All the results will evidence the cleavage mechanism yielding the photoacid generation of NIs.

Experimental and Methodology

Materials. The photoacid generators NIs [*N*-(nonafluorobutanesulfonyloxy)-1,8-naphthalimide (NIONf), *N*-(trifluoromethanesulfonyloxy)-1,8-naphthalimide (NIOTf), *N*-(methanesulfonyloxy)-1,8-naphthalimide (NIOMe), and *N*-(butanesulfonyloxy)-1,8-naphthalimide (NIOBu)] were provided by Midori Kagaku and recrystallized from chloroform. *N*-(*p*-Toluenesulfonyloxy)-1,8-naphthalimide (NIOTos) was synthesized according to a well-known procedure.[12,14] The acid sensor, tetrabromophenol blue sodium salt (TBPBNa), was purchased from Aldrich. All solvents were Aldrich and Fluka Spectrograde.

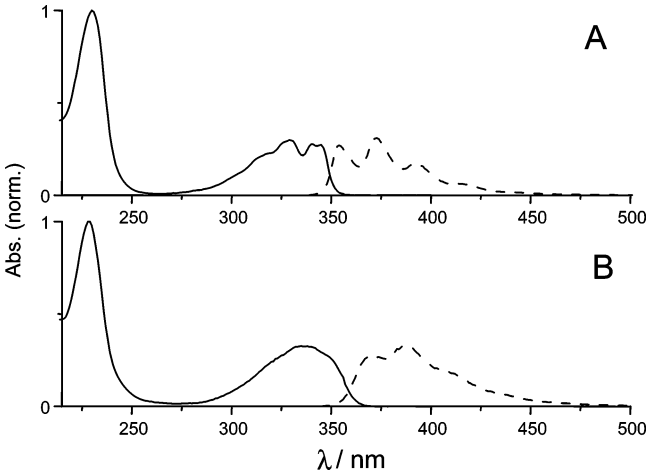

Figure 1. Absorption (plain line) and fluorescence (dots) spectra of NIOTf recorded in (A) hexane and (B) acetonitrile.

Experimental Procedures. A FluoroMax 2 Luminescence Spectrometer was used for the fluorescence and phosphorescence measurements. Fluorescence spectra were spectrally corrected. The fluorescence quantum yields were determined relatively to anthracene in ethanol ($\phi = 0.27$)[15] and were corrected for the solvent refractive index.

Steady state phosphorescence and emission anisotropy measurements (using Glan-Thompson polarizers) were perfomed in 2-methyltetrahydrofuran (2-MTHF) at 77 K. The samples are placed in a 5-mm diameter quartz tube in a

* Corresponding author. E-mail: x.allonas@uha.fr.
[†] Université de Haute Alsace.
[‡] Chiba University.

10.1021/jp0771926 CCC: $40.75
Published on Web 03/29/2008

SCHEME 1: Molecular Structures of NIs

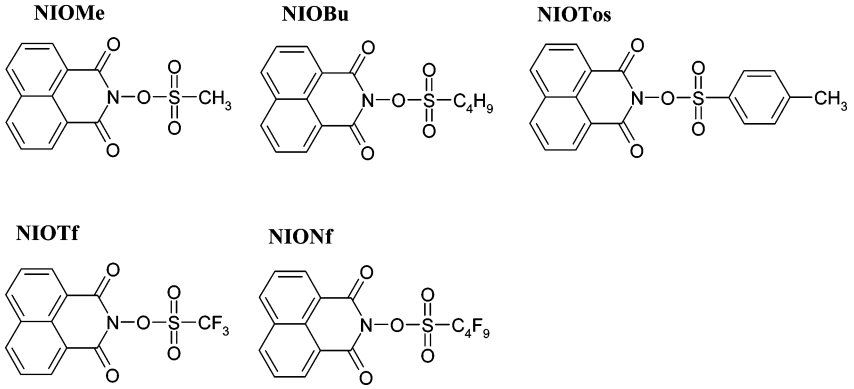

Dewar filled with liquid nitrogen. The anisotropy r is determined as

$$r = \frac{I_{VV} - gI_{VH}}{I_{VV} + 2gI_{VH}} \qquad \text{with } g = \frac{I_{HV}}{I_{HH}}$$

The subscripts denote the orientation of the excitation and emission polarizers (horizontal H or vertical V to the plane of the table), respectively. I is the emission intensity and g an instrumental correction factor.

The cyclic voltammetry experiments were performed at 300 K under nitrogen in acetonitrile with a constant concentration (0.1 M) of tetrabutylammonium tetrafluoroborate (*n*-Bu_4BF_4). Ferrocene was used as an internal reference. A computer-controlled Princeton 263A potentiostat in a three-electrode single-compartment cell was used. A saturated calomel electrode in methanol was placed in a separate compartment and used as a pseudoreference.

Laser Flash Photolysis (LFP) experiments were carried out on the nanosecond time scale with a Edinburgh Analytical Instruments LP900 equipped with a 450 W pulsed xenon arc lamp, a Czerny-Turner monochromator and a fast photomultiplier. The samples were irradiated with the third harmonic (λ = 355 nm, 10 ns pulse duration, 5 mJ per pulse) of a Nd/YAG (Powerlite 9010, Continuum). The sample concentration was adjusted to get an absorption of about 0.3 at the excitation wavelength.

The picosecond time-resolved absorption setup was based on a classical pump−probe arrangement using a picosecond laser as the excitation source. All the characteristics have been already reported elsewhere.[16] Determination of the intersystem crossing quantum yields ϕ_{isc} required a comparison with a standard system benzophenone/camphorquinone (BP/CQ). The CQ triplet is formed through a triplet−triplet energy transfer from BP; the optical density of the CQ triplet reaches a plateau value when most of the BP triplet states are quenched. Assuming that the plateau value corresponds to a 100% efficiency for the energy transfer, the ϕ_{isc} values are determined according to the following equation:

$$\frac{\Phi_{ISC}^{BP}}{\Phi_{ISC}^{NI}} = \frac{\Delta OD^{BP}}{\Delta OD^{NI}}$$

where ϕ_{isc}^{BP} and ϕ_{isc}^{NI} are the intersystem crossing quantum yields of BP (which is equal to unity) and NI, respectively. ΔOD^{BP} and ΔOD^{NI} are the maximum optical density of the CQ triplet for the system BP/CQ and NI/CQ, respectively. The change in the optical density was investigated by varying the CQ concentrations up to the limit where CQ itself absorbs the excitation light. The triplet state of CQ was monitored at 800 nm.[17] The concentrations of each donor were carefully adjusted to have the same absorbance at 355 nm.

TABLE 1: Photophysical and Electronic Properties of the Naphthalimide Ground States

	hexane	acetonitrile		
	λ^{max}_{abs}/ nm	λ^{max}_{abs}/ nm	ϵ^{max}/M^{-1} cm^{-1} [a]	E_{red}/ V vs SCE
NIOTf	329	335	10150	−0.95
NIOMe	329	333	13380	−1.05
NIONf	329	334	14570	−0.95
NIOBu	329	332	12830	−1.05
NIOTos	328	332	16170	−1.02

[a] Lowest energy electronic band.

TABLE 2: Photophysical Properties of the Naphthalimides Singlet States in Hexane and in Acetonitrile

	hexane				acetonitrile		
	λ^{max}_{fluo}/ nm	ϕ_{fluo}	ϕ_{ISC}	E_a/ kcal mol^{-1}	λ^{max}_{fluo}/ nm	ϕ_{fluo}	ϕ_{ISC}
NIOTf	368	0.13	0.90	2.71	383	0.07	0.12
NIOMe	369	0.02	1	1.66	382	0.28	0.52
NIONf	369	0.13	0.91	2.15	384	0.06	0.12
NIOBu	368	0.01	1	1.45	382	0.25	0.45
NIOTos	368	0.02	*a*	0.45	381	0.34	0.49

[a] Insoluble above 5×10^{-5} M.

The photoacid generation quantum yields were determined by using TBPBNa as the acid sensor.[18] The third harmonic of the Nd:YAG laser was used. TBPBNa was added after the laser irradiation. The photoacid generation leads to a decrease of the maximum absorbance of TBPBNa. By using a calibration curve, the amount of the photogenerated acids was evaluated.

Optimization of the geometrical structures, excited states energies and bond dissociation energies were calculated using the density functional theory[19] at the B3LYP/6-31* level. Time-dependent calculations were performed at the TDB3LYP/6-311++G** to obtain information about the spectrocopic excited states.

Results and Discussion

Ground and Excited Singlet State Properties. All the NIs exhibit similar absorption and steady state fluorescence spectra, and Figure 1 shows the ones corresponding to NIOTf. Tables 1 and 2 present relevant spectroscopic and energetic data. Each absorption spectrum exhibits an intense band in the 220−290 nm range and a lower intensity band located between 310 and 370 nm: no important effects of the substitution are noted. The

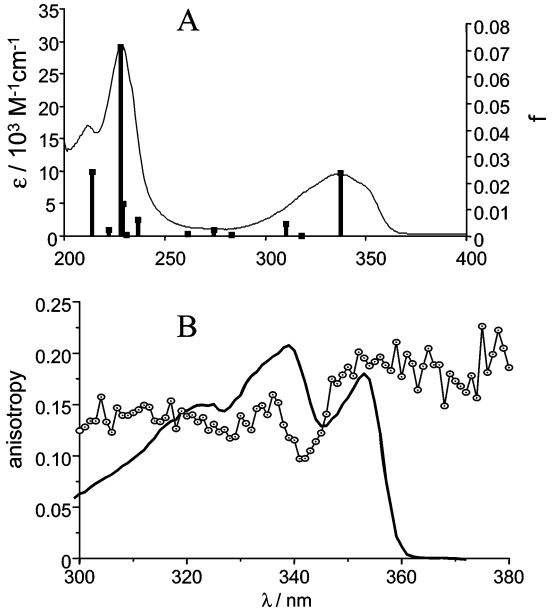

Figure 2. (A) Experimental absorption spectrum of NIOTf in acetonitrile and computed electronic S_0-S_n transitions. (B) Excitation spectrum and anisotropy excitation spectrum of NIONf measured in glassy 2-MTHF.

wavelengths of the singlet state electronic transitions were computed using a time-dependent DFT procedure at the TDB3LYP/6-311++G** on a B3LYP/6-31G* optimized ground state. Figure 2A underlines the excellent agreement between the calculated absorption spectrum and the experimental one obtained in acetonitrile, giving confidence to the procedure used. These calculations show that the lowest energy band mainly consists in the overlapping of three electronic transitions with different oscillator strengths f.

Both LUMO and HOMO are typical π orbitals delocalized on the carbon and oxygen atoms of the naphthalimide cycle. The S_0-S_1 transition is mainly a HOMO−LUMO transition and consequently the oscillator strength is very high ($f = 0.024$). This is in line with the high extinction coefficient measured for NIOTf. The predicted transition energy corresponds to a maximum located at 337.4 nm (84.8 kcal/mol), in very good agreement with the experimental value. On the contrary the S_0-S_2 transition predicted at 318.3 nm (89.9 kcal/mol) is a pure $HOMO_{-2}$-LUMO transition which is symmetry forbidden. This can be attributed to the fact that $HOMO_{-2}$ is a pure n orbital with a large contribution of the lone pairs of both the oxygen atoms of the naphthalimide cycle. Consequently, the S_0-S_2 transition has a $n\pi^*$ nature and the oscillator strength is almost zero. Finally, the S_0-S_3 transition has a $\pi\pi^*$ nature (311 nm, 92.04 kcal/mol, $f = 0.0045$). Only the former and the latter have significant oscillator strengths. Therefore, one can consider that the lowest energy absorption band consists of the S_0-S_3 transition in its blue tail to the S_0-S_1 transition in the red tail.

These computations are in very good agreement with the fluorescence excitation and anisotropy spectra for NIONf in a frozen solution of 2-MTHF (77 K) displayed in Figure 2B. The observed anisotropy behaves similarly for all naphthalimide compounds and reaches a plateau above 350 nm with an average value of 0.185. The anisotropy value drops down between 340 and 345 nm and a value of 0.136 was found for the 300−340 nm region. This result is consistent with the existence of an overlapping between at least two electronic transitions. In fact, the low energy absorption band of the 1,8-naphthalimides mainly consists of two electronic transitions referred as $S_0-{}^1L_a$ and

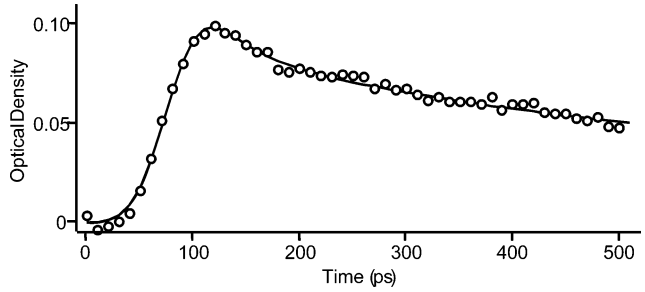

Figure 3. Kinetic treatment of the buildup and decay of the S_1 state absorption of NIOTf in acetonitrile at 450 nm (picosecond laser irradiation at 355 nm) according to the a scheme involving two excited singlet states. Open circles: experimental data. Full line: theoretical fit.

$S_0-{}^1L_b$ (Platt labels) which are respectively polarized along the C_2 axis of the 1,8-naphthalimide molecule and in the plane perpendicular to the C_2 axis.[20] The anisotropy of the $S_0-{}^1L_a$ band exhibits a value noticeable smaller than the theoretical value obtained for an electronic transition colinear with the absorption transition moment. Both transitions are hardly affected by the solvent polarity with a slight red shift from hexane to acetonitrile (ca. +6 nm), a fact that emphasizes the weak polar character of the ground state.

The excited singlet state absorption was previously followed by picosecond laser spectroscopy[13] but the kinetic treatment was not completely supported. According to the presence of the two close lying excited singlet states mentioned above, the build up and the decay of this absorption can now be correctly fitted (Figure 3), confirming the presence of at least two excited singlet states. A simplified scheme for the decay calculation is shown in Scheme 2.

The best fit was found for the following set of parameters: $1/k_{ic} = 38$ ps, $1/k_{isc} = 10$ ps (within the time resolution of the apparatus) and $1/k_a = 520$ ps corresponding to the singlet state fluorescence lifetime; $k_a = k_{ic} + k_{isc} + k_f$.

All the NIs used in this work behave similarly to NIOTf. The substitution effect is almost imperceptible on the shape of the last absorption band. Moreover, the extinction coefficients of all naphthalimides have similar values, indicating that the substituents on the nitrogen atom do not significantly affect the photophysical properties of the naphthalimide moiety in the singlet ground state.

In a given solvent, the fluorescence spectra of all NIs are similar with a maximum emission located at 380 nm in acetonitrile. The zero−zero transition lies at approximately 360 nm giving a singlet energy of 79.5 kcal/mol. Increasing the solvent polarity leads to a red shift of the emission band, which does not exceed 15 nm. Each spectrum kept its vibronic structure with a half-maximum full width insensitive to the solvent polarity. The mirror image relationship observed between the fluorescence and the long-wavelength absorption spectra indicates that the geometries of both the ground and excited states are similar. The change in the dipole moment between the ground and excited state $\Delta\mu_{g-s}$ can be estimated from the $\Delta\nu_{max}$ difference between the absorption and fluorescence maximum on the basis of the Lippert's Δf function[21] under the assumption that the Onsager cavity has a radius of 4.3 Å.[22] Whatever the naphthalimide derivative considered, the change of this dipole moment hardly reaches 5 D. Therefore, the singlet excited state exhibits a very weak polar character, which suggests that an heterolytic cleavage of the N−O bond should not be favored.

Such a weak solvent effect on the fluorescence spectra singularly contrasts with the decrease of the corresponding

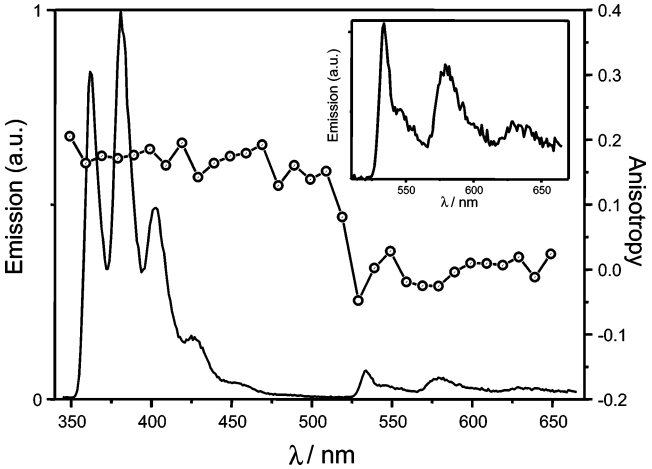

Figure 4. Fluorescence, phosphorescence and anisotropy emission spectra of NIOMe in a glassy matrix of 2-MTHF.

TABLE 3: Photophysical Properties of the Naphthalimides Triplet States in Glassy Matrix of 2-MTHF

	λ^{max}_{fluo}/ nm	λ^{max}_{phos}/ nm	E_T/ kcal mol^{-1}	Δ_{S-T}/ kcal mol^{-1}
NIOTf	381	534−582-635	53.4	21.4
NIOMe	381	536−581-634	53.2	21.6
NIONf	378	534−582-635	53.3	22.1
NIOBu	377	536−582-634	53.2	22.4
NIOTos	377	535−581-634	53.3	22.3

emission quantum yields ϕ_f when decreasing the solvent polarity. For instance, considering the NIs bearing nonperfluorated substituents, the fluorescence quantum yield is at least divided by a factor 10 when going from hexane to acetonitrile, a fact that will be discussed below.

All the NIs show fully reversible voltamogramms in acetonitrile; a decrease of the reduction potential is observed when going from alkyl to perfluoalkyl substituents. The radical anion that is generated is all the more stabilized that the substituents have a (−I) electronic effect. The reduction potentials are almost not affected by the substitution.

Triplet State Properties. The phosphorescence emission of naphthalimides were collected in glassy matrixes of 2-MTHF at 77 K and the corresponding spectroscopic data are given in Table 3. Figure 4 shows the normalized phosphorescence spectra of NIONf. The phosphorescence spectrum in 2-MTHF, observed in the 550−650 nm region, is well structured. Whatever the NIs studied, the shapes of the phosphorescence spectra are similar and the measured triplet energies are almost constant. The substituents have almost no effect on the electronic properties of the triplet states. Moreover, these spectra are also perfectly comparable with the spectra of other 1,8-naphthalimide derivatives bearing other different substituents.[23] This therefore confirms that the electronic excitation is well centered on the naphthalimide moiety. The measured phosphorescence lifetimes are in the range of 0.5 s, thereby indicating a π,π^* character for the lowest lying T_1 state: this state is populated from the n,π^* triplet state mentioned above. The steady state emission anisotropy spectrum, displayed in Figure 4, exhibits a significant change when going from the fluorescence to the phosphorescence region (the mean anisotropy value decreases from +0.17 to −0.03). This leads to a tilt angle of 20° between the fluorescence and the phosphorescence dipole moments, indicating a change of the charge symmetry after the intersystem crossing process.

These conclusions are nicely confirmed by time-dependent DFT calculations performed at the TDB3LYP/6-311++G** level on the ground state geometry optimized at the B3LYP/6-31G* level. Indeed, The S_0-T_1 transition is predicted to be $\pi\pi^*$ nature with an energy of 63.4 kcal/mol (535 nm), in excellent agreement with the phosphorescence results. Interestingly, a S_0-T_2 transition was found to have an energy of 76.1 kcal/mol and to also exhibit a $\pi\pi^*$ nature whereas a nπ^* S_0-T_3 transition was found to be very close in energy (83.3 kcal/mol) to that of the S_0-S_1 one. All these results allow us to draw an energy diagram for the different excited states of NIs (Figure 5).

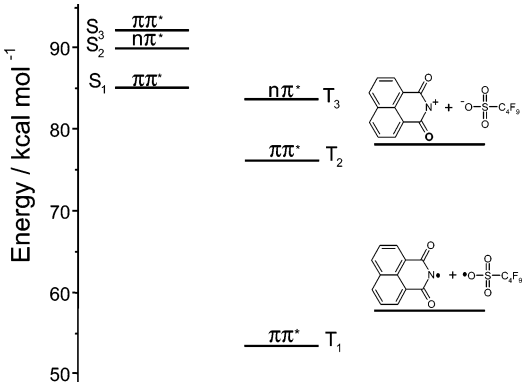

Figure 5. Computed energy levels for NIOTf.

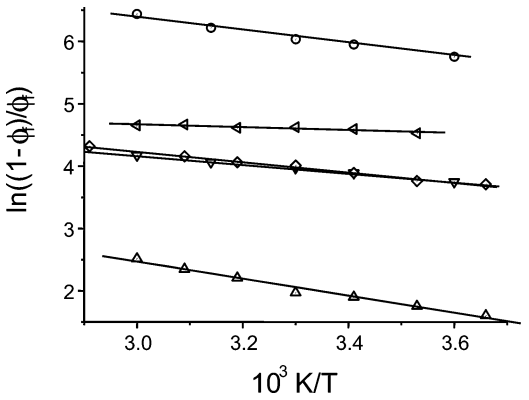

Figure 6. Plot of $\log[(1-\phi_f)/\phi_f]$ vs $1/T$ for naphthalimide derivatives in hexane. See text.

The intersystem crossing quantum yields behave in an opposite way than the fluorescence quantum yield. Indeed, the former strongly increases when decreasing the solvent polarity and appears as the major deactivation pathway of the S_1 state (Table 2). In a nonpolar solvent, fluorescence and intersystem crossing pathways alone account for the whole singlet excited state deactivation. Therefore, the following relationship can be derived:

$$\frac{k_{ISC}}{k_{fluo}} = \frac{1-\Phi_{fluo}}{\Phi_{fluo}}$$

where k_{fluo} and k_{isc} correspond to the rate constants of the fluorescence emission and intersystem crossing respectively. Only k_{isc} is temperature dependent, and under the assumption of an Arrhenius relationship, the activation energy E_a of the intersystem crossing process can be easily measured by a temperature effect. The plots displayed in Figure 6 lead to E_a (Table 2). In all cases, this activation energy does not exceed 3 kcal/mol. Indeed, the photophysical properties of the S_1 state of these NIs are mainly controlled by the presence of a close-lying n,π^* triplet excited state (as already reported for naphthalimide itself[24,25]) which explains the high intersystem crossing

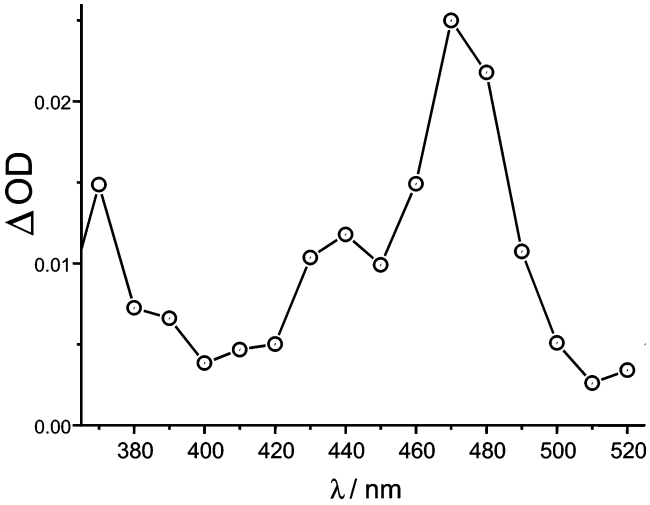

Figure 7. Transient absorption spectrum of NIOTf in acetonitrile recorded 3 μs after the laser pulse.

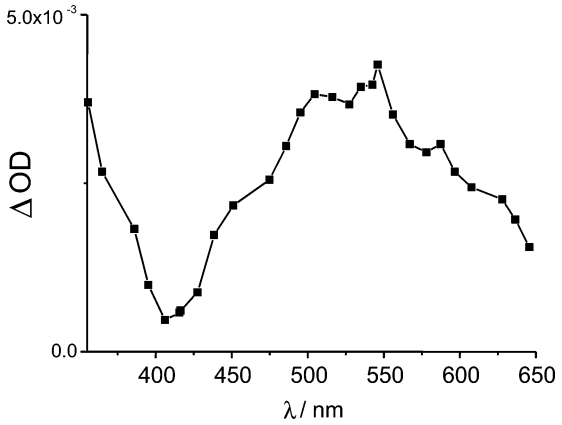

Figure 8. Transient absorption spectrum of NIOTos in aerated acetonitrile obtained 0.6 μs after the laser pulse.

efficiency. Due to the acid formation in polar solvents, the measurement of E_a is not possible in acetonitrile.

Triplet−triplet absorption spectra of the NIs in degassed acetonitrile have been obtained by direct laser excitation at 355 nm. A typical transient absorption spectrum is presented in Figure 7, which exhibits a maximum at 470 nm with a shoulder at 440 nm. For all NIs, the triplet lifetime is a few tens of microseconds, showing that the acid formation does not proceed from the triplet state. These spectroscopic data are in good agreement with the previously studied 1,8-naphthalimide chromophores.[24,26,27] In oxygen saturated solution, the triplet state is strongly quenched. The new additional large transient spectrum observed in the 450−650 nm range for NIOTos (Figure 8) is similar to that reported for the transient absorption spectra of the *p*-toluenesulfonyl radical originating from some oxime type PAG[10] and is consequently attributed to *p*-tolueneoxysulfonyl radical. As observed in the literature,[10] the transient decay mainly obeys to a first-order kinetic (transient lifetime: 7.5 μs). The presence of this radical is a direct evidence for the homolytic N−O bond cleavage of NIOTos.

Photolysis and Photoacid Generation. Laser excitation at 355 nm leads to a profound modification of the absorption and fluorescence spectrum in acetonitrile as shown in Figure 9: the absorption bands of NIONf located at 335 nm and at 227 nm are strongly decreased and three new bands progressively appear at 211, 250 and 360 nm. The four isosbestic points are in favor of an equilibrium reaction. In the same way, the fluorescence band continuously decreased and a new intense large band with

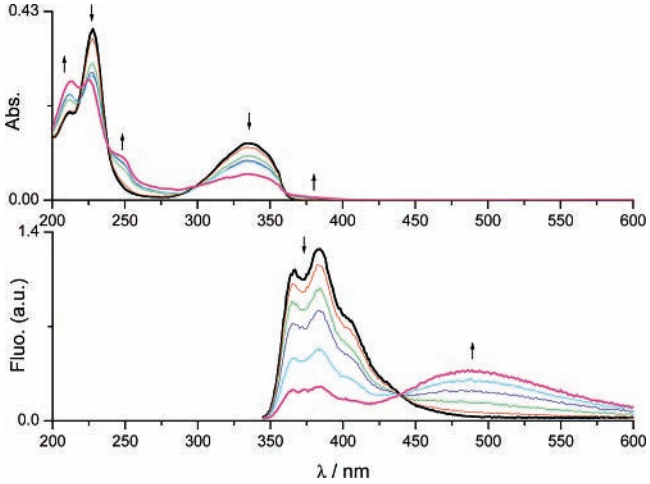

Figure 9. Evolution of the absorption (A) and fluorescence emission (B) of NIONf upon laser irradiation at 355 nm.

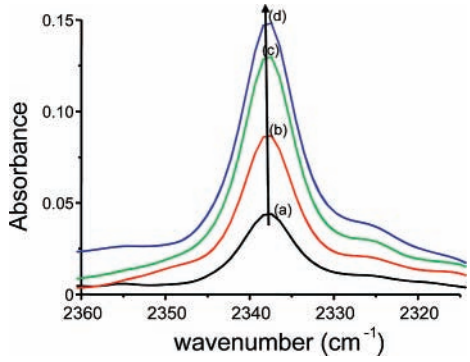

Figure 10. Growth of the new infra red band at 2337 cm^{-1} upon laser irradiation at 355 nm of NIONf in CH_2Cl_2. Irradiation time: (a) 3 min, (b) 9 min, (c) 20 min, (d) 40 min.

a maximum at 480 nm arose in the red region. The isoemissive point observed at 430 nm suggests the occurrence of a photochemical reaction in the excited singlet state that yields a new fluorescent product. This product has been assigned to benz[*cd*]indol-2(1*H*)-one (BIONE) whose both emission and excitation spectra strikingly coincide with the photophysical fingerprint of the photoproduct.[13] On the other hand, the photoconversion of the NIs in ethanol which is followed-up through fluorescence leads to a new product whose emission spectrum is strongly blue-shifted compared to the BIONE emission.

During the photoreaction in acetonitrile, CO_2 is produced as shown by its characteristic infra red band located at 2337 cm^{-1} (Figure 10). In the same conditions, in ethanol, CO_2 release is not detected any more. It was already suggested[28] that the photoproducts in ethanol and acetonitrile are different besides the fact that the photoconversion quantum yield drops from 0.17 in acetonitrile to 0.07 for NIOTf in ethanol.

Finally, the role of water was also emphasized. Actually, after reaching a stationary regime during the photoconversion of a highly concentrated solution of NIONf in acetonitrile, the addition of an aliquot of water reinitiated the acid production (as previously reported for NIOTf[13]).

In acetonitrile, the sum of the fluorescence and intersystem quantum yield, is higher than 0.8 for a nonfluorinated NIs whereas it decreases below 0.2 for a perfluorinated NIs. Assuming that the cleavage process is the third deactivation pathway in polar solvent, it appears that the maximum value of the cleavage quantum yield of NIOTf and NIONf in acetonitrile is c.a. 0.8 and about 0.2−0.3 for NIOMe, NIOBu and NIOTos.

TABLE 4: Acid Generation Quantum Yields in Naphthalimides in Acetonitrile

	NIOTf	NIOMe	NIONf	NIOBu	NIOTos
ϕ_{acid}	0.18	0.02	0.23	0.02	0.04

TABLE 5: Singlet and Triplet States Energies, Bond Dissociation Energy for the N−O Bond Heterolytic and Homolytic Cleavage

	E_S/ kcal mol^{-1}	E_T/ kcal mol^{-1}	BDE(hetero)/ kcal mol^{-1}	BDE(homo)/ kcal mol^{-1}
NIOTf	80.4	57.5	78.1	57.8
NIOMe	80.7	57.3	101.7	59.6
NIONf	80.4	57.3	75.4	58.4
NIOBu	80.7	57.0	102.0	59.1
NIOTos	80.4	57.5	99.1	57.9

SCHEME 2: Simplified Scheme for Fitting the Picosecond Absorption Decay

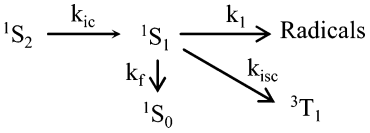

The photoacid generation quantum yields ϕ_{acid} were determined in acetonitrile (Table 4). Nonperfluorated naphthalimides present very low photoacid quantum yields (below 0.05) whereas perfluorated derivatives exhibit a more significant values (about 0.2). However, in nonpolar solvent, all ϕ_{acid} collapse dramatically. It appears that the high ϕ_{acid} are in line with the low ϕ_{fluo} and ϕ_{ISC} values, suggesting again that the acid generation occurs from the excited singlet state.

Cleavage Mechanism. The bond dissociation energy (BDE) and the lowest singlet E_S and triplet E_T states energy were calculated by the DFT method for both the hypothetical homolysis and heterolysis cleavages (Table 5). These calculations were performed by calculating the energy difference between the optimized and separated products and the NI ground state (Figure 5). The absence of any effect of the chemical structure on E_S and E_T values as well as the $E_S - E_T$ difference are in good agreement with the experimental observations. In any case, the N−O bond cleavage from the lowest triplet state is an endergonic process and therefore should not take place. The singlet state homolysis is clearly exergonic. The calculated BDEs for the heterolysis suggest that they are too high to be operative: the BDE value was calculated to be close to the nπ^* triplet state energy but the internal conversion between the nπ^* and $\pi\pi^*$ triplet state is presumably more efficient than a heterolytic cleavage process. These calculations confirm that a homolytic cleavage occurs from the excited singlet states.

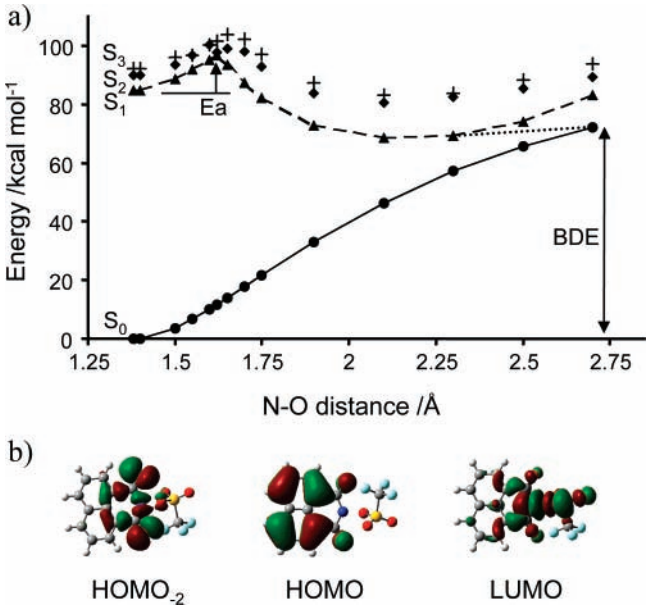

Figure 11. (a) Potential energy surface of NIOTf and (b) orbitals involved in the S_1 and S_2 excited states at a distance of 1.700 Å.

Potential energy surfaces (PES) for the cleavage process can be computed by optimizing the ground state structure of NIOTf at the B3LYP/6-31G* level, keeping the N−O bond length

SCHEME 3: Proposed Mechanism of the Acid Photogeneration in Perfluorinated Naphthalimides

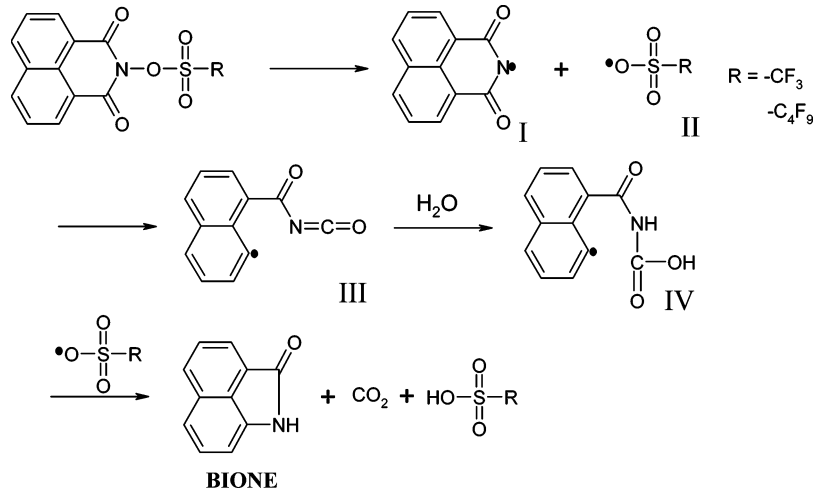

SCHEME 4: Alternative Cleavage Reaction Route in Ethanol

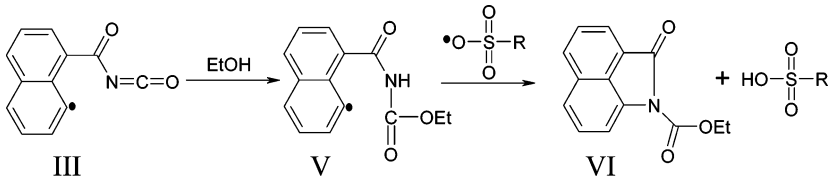

constrained at given values. Then, on each optimized structure, a TDB3LYP/6-311++G** was performed, leading to the energy values of the S_0, S_1, S_2 and S_3 states at each N−O distance value. The resulting PES for NIOTf is given Figure 11. The equilibrium N−O distance was found at 1.3825 Å. Increasing this distance leads to an increase of the ground state energy up to the complete dissociation at a distance higher than 2.7 Å. Interestingly, the PES corresponding to the excited singlet states behave similarly up to a distance of about 1.62 Å. Then, the cleavage reaction occurs in the excited states and a transition state was found. Although the program used does not allow us to optimize this transition state, a value of about 12 kcal/mol was found as activation energy on the S_1 surface. For N−O bond lengths higher than 1.62 Å, the energy of the excited singlet states decreases slightly, leading to the formation of radicals. This kind of scheme is typical for the crossing of $\pi\pi^*$ or $n\pi^*$ states with $\sigma\sigma^*$ states that are dissociatives.[29]

It can be clearly seen in Figure 11 that there is a crossing point between the S_1 and the S_2 states. This confirms the involvement of the S_2 excited state in the photodissociation process of NIs. The orbitals involved are shown in Figure 11. Close to the transition state (at a distance of 1.700 Å) the S_1 excited state corresponds clearly to a $\pi\sigma^*$ HOMO−LUMO excitation, the LUMO being clearly a dissociative σ^* orbital; interestingly, the S_2 excited singlet is mainly a $n\sigma^*$ HOMO−2−LUMO excitation. As a consequence, there is therefore no doubt about the dissociative nature of the S_1 and S_2 PES. However, it seems that the formation of the S_1 state from S_2 is strongly favored compared to the direct dissociation from S_2: this supports the proposed Scheme 2.

All these results are consistent with the overall mechanism recently proposed for NIOTf[13] and briefly recalled in Scheme 3 for the acid production. The homolytic cleavage of the N−O bond in the singlet excited state leads to both a production of a naphthalimide radical I and a perfluorobutanesulfonyl radical II. The radical I then undergoes a ring-opening reaction to generate an isocyanate radical intermediate III. The formation of intermediate such as III from imidyl radical (i.e., I) has been discussed in details elsewhere.[30] In the presence of residual water, III is hydrolyzed leading to the formation of a carbamic acid derivative IV. Hydrogen abstraction between II and IV is followed by CO_2 release and BIONE formation, a process that is expected to be exergonic by virtue of the decarboxylation process.

In ethanol, the mechanism may be slightly different. It involves an alternative reaction route where the isocyanate radical intermediate III reacts with ethanol leading to a carbamate radical derivative V (Scheme 4).

Subsequent hydrogen abstraction should require a homolytic N−H bond cleavage of the carbamate group V followed by a ring closure VI. In this step, the hydrogen abstraction occurring between the sulfonyl radical and the N−H group is a more endergonic process compared to that occurring with the carboxylic group in a polar solvent: this explains the observed decrease of the photoconversion quantum yield.

Conclusion

The photophysical properties of a new series of 1,8-naphthalimides bearing different substituents (alkyl, perfluoroalkyl, aryl moieties) were analyzed and discussed. These substituents do not significantly affect the singlet and triplet states energy levels, indicating that the excitation is mainly located on the 1,8-naphthalimide moiety. In polar solvents, NIs bearing perfluoroalkyl substituents exhibit a significant singlet N−O bond cleavage that competes with the intersystem crossing process. The overall mechanism leading to the acid depends on the presence of residual amount of water or alcohol.

References and Notes

(1) Ito, H.; Willson, C. G. In *Polymers in Electronics*; Davidson, T., Ed.; ACS Symposium Series; American Chemical Society: Washington, DC, 1984; Vol. 242.

(2) Ito, H.; Willson, C. G.; Fréchet, J. M. J.; Farall, M. H.; Eichler, E.; *Macromolecules* **1983**, *16*, 510.

(3) Fouassier, J. P.; Rabek, J. F. *Radiation Curing in Polymer Science and Technology*; Elsevier: Amsterdam, 1983.

(4) Andraos, J.; Barclay, G. G.; Medeiros, D. R.; Baldovi, M. V.; Scaiano, J. C.; Sinta, R. *Chem. Mater.* **1998**, *10* (6), 1694−1699.

(5) Iwaki, J.; Suzuki, S.; Park, C.; Miyagawa, N.; Takahara, S.; Yamaoka, T. *J. Photopolym. Sci. Technol.* **2004**, *17* (1), 123−124.

(6) Okamura, H.; Sakai, K.; Tsunooka, M.; Shirai, M.; Fujiki, T.; Kawasaki, S.; Yamada, M. *J. Photopolym. Sci. Technol.* **2003**, *16* (1), 87−90.

(7) Ortica, F.; Coenjarts, C.; Scaiano, J. C.; Liu, H.; Pohlers, G.; Cameron, J. F. *Chem. Mater.* **2001**, *13* (7), 2297−2304.

(8) Suzuki, S.; Allonas, X.; Fouassier, J.-P.; Urano, T.; Takahara, S.; Yamaoka, T. *J. Photochem. Photobiol. A* **2006**, *181*, 60−66.

(9) Ortica, F.; Scaiano, J. C.; Pohlers, G.; Cameron, J. F.; Zampini, A. *Chem. Mater.* **2000**, *12* (2), 414−420.

(10) Arnold, P. A.; Fratesi, L. E.; Bejan, E.; Cameron, J.; Pohlers, G.; Liu, H.; Scaiano, J. C. *Photochem. Photobiol. Sci.* **2004**, *3*, 864−869.

(11) Coenjarts, C.; Garcıa, O.; Llauger, L.; Palfreyman, J.; Vinette, A. L.; Scaiano, J. C. *J. Am. Chem. Soc.* **2003**, *125*, (3), 620−621.

(12) Iwashima, C.; Imai, G.; Okumara, H.; Tsunooka, M.; Shirai, M. *J. Photopolym. Sci. Technol.* **2003**, *16*, 91.

(13) Malval, J. P.; Morlet-Savary, F.; Allonas, X.; Fouassier, J.-P.; Suzuki, S.; Takahara, S.; Yamaoka, T. *Chem. Phys. Let.* **2007**, *443* (4−6), 323−327.

(14) Narita, M.; Teramoto, T.; Okawara, M. *Bull. Chem. Soc. Jpn.* **1971**, *44*, 1084.

(15) Melhuish, W. H. *J. Phys. Chem.* **1961**, *65* (2), 229−235.

(16) Morlet-Savary, F.; Ley, C.; Jacques, P.; Fouassier, J. P. *J. Phys. Chem. A* **2001**, *105*, 11026.

(17) Allonas, X.; Fouassier, J.-P.; Angiolini, L.; Caretti, D. *Helv. Chim. Acta* **2001**, *84*, 2577.

(18) Shah, M.; Allen, N. S.; Salleh, N. G.; Corrales, T.; Egde, M.; Catalina, F.; Bosch, P.; Green, A. *J. Photochem. Photobiol. A* **1997**, *111*, 229−232.

(19) Frisch, M. J.; Trucks, G. W.; Schlegel, H. B.; Scuseria, G. E.; Robb, M. A.; Cheeseman, J. R.; Zakrzewski, V. G.; Montgomery, J. A., Jr.; Stratmann, R. E.; Burant, J. C.; Dapprich, S.; Millam, J. M.; Daniels, A. D.; Kudin, K. N.; Strain, M. C.; Farkas, O.; Tomasi, J.; Barone, V.; Cossi, M.; Cammi, R.; Mennucci, B.; Pomelli, C.; Adamo, C.; Clifford, S.; Ochterski, J.; Petersson, G. A.; Ayala, P. Y.; Cui, Q.; Morokuma, K.; Malick, D. K.; Rabuck, A. D.; Raghavachari, K.; Foresman, J. B.; Cioslowski, J.; Ortiz, J. V.; Stefanov, B. B.; Liu, G.; Liashenko, A.; Piskorz, P.; Komaromi, I.; Gomperts, R.; Martin, R. L.; Fox, D. J.; Keith, T.; Al-Laham, M. A.; Peng, C. Y.; Nanayakkara, A.; Gonzalez, C.; Challacombe, M.; Gill, P. M. W.; Johnson, B. G.; Chen, W.; Wong, M. W.; Andres, J. L.; Head-Gordon, M.; Replogle, E. S.; Pople, J. A. *Gaussian 98*, revision A.11; Gaussian, Inc.: Pittsburgh, PA, 1998.

(20) Gawronski, J.; Gawronska, K.; Skowronek, P.; Holmen, A. *J. Org. Chem.* **1999**, *64* (1), 234−241.

(21) Lippert, E. *Z. Electrochem.* **1957**, *61*, 962.

(22) Demeter, A.; Berces, T.; Biczok, L.; Wintgens, V.; Valat, P.; Kossanyi, J. *J. Phys. Chem.* **1996**, *100* (6), 2001−2011.

(23) Kolosov, D.; Adamovich, V.; Djurovich, P.; Thompson, M. E.; Adachi, C. *J. Am. Chem. Soc.* **2002**, *124* (33), 9945−9954.

(24) Wintgens, V.; Valat, P.; Kossanyi, J.; Biczok, L.; Demeter, A.; Berces, T. *J. Chem. Soc., Faraday Trans.* **1994**, *90* (3), 411−421.

(25) Demeter, A.; Berces, T.; Biczok, L.; Wintgens, V.; Valat, P.; Kossanyi, J. *J. Chem. Soc., Faraday Trans.* **1994**, *90* (18), 2635−2641.

(26) Samanta, A.; Ramachandram, B.; Saroja, G. *J. Photochem. Photobiol. A* **1996**, *101*, 29−32.

(27) Dijk, S. I. v.; Groen, C. P.; Hartl, F.; Brouwer, A. M.; Verhoeven, J. W. *J. Am. Chem. Soc.* **1996**, *118* (35), 8425−8432.

(28) Saotome, M.; Takano, S.; Tokushima, A.; Ito, S.; Nakashima, S.; Nagasawa, Y.; Okada, T.; Miyasaka, H. *Photochem. Photobiol. Sci.* **2005**, *4*, 83−88.

(29) Allonas, X.; Morlet-Savary, F.; Lalevée, J.; Fouassier, J. P. *Photochem. Photobiol.* **2006**, *82*, 88.

(30) Kasai, P. H. *J. Am. Chem. Soc.* **1992**, *114*, 2875−2880.